MTCL2 is a new Golgi-resident microtubule-regulating protein, essential for organizing asymmetric microtubule network

Risa Matsuoka†, Masateru Miki†, Sonoko Mizuno, Yurina Ito, Atsushi Suzuki*

Molecular Cellular Biology Laboratory, Yokohama City University Graduate School of Medical Life Science, 1-7-29 Suehiro-cho, Tsurumi-ku, Yokohama 230-0045, Japan

† These authors contributed this work equally.

* Corresponding author: Atsushi Suzuki
1-7-29, Suehiro-cho, Tsurumi-ku, Yokohama 230-0045, Japan
TEL: 045-508-7238; E-mail: abell@tsurumi.yokohama-cu.ac.jp

Running title: MTCL2 is a novel microtubule-regulating protein

Keywords: MTCL1, SOGA, Golgi ribbon, microtubule, polarity

Abstract

The Golgi apparatus plays important roles in organizing the asymmetric microtubule network essential for polarized vesicle transport. The Golgi-associated coiled-coil protein MTCL1 is crucially involved in Golgi functioning by interconnecting and stabilizing microtubules on the Golgi membrane through its N- and C-terminal microtubule-binding domains. Here, we report the presence of a mammalian paralog of MTCL1, named MTCL2, lacking the N-terminal microtubule-binding domain. MTCL2 localizes to the Golgi membrane through the N-terminal region and directly binds microtubules through the conserved C-terminal domain without promoting microtubule stabilization. Knockdown experiments demonstrated essential roles of MTCL2 in accumulating MTs around the Golgi and regulating the Golgi ribbon structure. *In vitro* wound healing assays further suggested a possible intriguing activity of MTCL2 in integrating the centrosomal and Golgi-associated microtubules around the Golgi ribbon, thus supporting directional migration. Altogether, the present results demonstrate that cells utilize two members of the MTCL protein family to differentially regulate the Golgi-associated microtubules for controlling cell polarity.

Introduction

The microtubule (MT) cytoskeleton plays essential roles in organizing intracellular structures by mediating the transport and positioning of organelles. Generally, in animal cells MTs radiate from the centrosome, where MT nucleation and attachment of MT minus ends occur predominantly (Conduit et al., 2015; Vorobjev and Nadezhdina, 1987). However, the presence of other subsets of MTs that lack centrosome anchoring (non-centrosomal MTs) has been documented over the last decade and their physiological significance has received considerable attention from cell biologists (Akhmanova and Hoogenraad, 2015; Bartolini and Gundersen, 2006; Nishita et al., 2017). In particular, non-centrosomal MTs appear in differentiated cells, such as epithelial, neuronal, or skeletal muscle cells, where the centrosome loses its MT nucleation activity (Muroyama and Lechler, 2017). Contrasting to centrosomal MTs, which exhibit dynamic instability at their plus ends and radiate rather symmetrically, non-centrosomal MTs are stabilized by mechanisms that are not completely clarified (Baas et al., 2016; Pepperkok et al., 1990), and are frequently bundled and organized into cell-type specific arrays that support cell polarization (Bacallao et al., 1989; Hahn et al., 2019; Mogensen et al., 1989; Oddoux et al., 2013). Recent studies have revealed that less differentiated cultured cells containing centrosomal MTs can also develop non-centrosomal MTs (Meiring et al., 2020). The most intensely studied non-centrosomal MTs of this kind are the Golgi-associated MTs, which nucleate from or attach their minus ends to the Golgi membrane (Efimov et al., 2007; Rivero et al., 2009; Wu et al., 2016). These MTs are stabilized and asymmetrically accumulated around the Golgi as dense networks (Chabin-Brion et al., 2001), and connect the individual Golgi stacks laterally (Miller et al., 2009). As a result, these Golgi-

43 associated MTs facilitate the formation of vertebrae-specific, crescent-like assembly of
44 Golgi stacks, called the Golgi ribbon, which is required for the polarization of vesicle
45 transport and thus directional migration (Wei and Seemann, 2010; Yadav et al., 2009).
46 The molecular mechanisms by which Golgi-associated MTs nucleate from or attach
47 their minus ends to the Golgi membrane have been intensely studied (Wu and Akhmanova,
48 2017; Wu et al., 2016; Yang et al., 2017). However, how these MTs are specifically
49 stabilized and accumulated remained unclear until recently, when we identified a novel
50 MT-regulating protein named MTCL1 (microtubule crosslinking factor 1) (Sato et al.,
51 2013; Sato et al., 2014). MTCL1 is an MT lattice-binding protein that specifically
52 condenses to the Golgi membrane and plays essential roles in the cross-linkage and
53 stabilization of Golgi-associated microtubules. MTCL1 is a long coiled-coil protein with
54 two MT-binding domains (MTBDs) at the N- and C-terminal regions. The C-terminal
55 MTBD (C-MTBD) has the ability to stabilize the polymerization state of MTs, and was
56 shown to be essential for specific stabilization of Golgi-associated MTs (Abdul Kader et
57 al., 2017; Sato et al., 2014). In contrast, the N-terminal MTBD (N-MTBD) of MTCL1,
58 binds MTs without affecting their stability and induces MT bundling only when it
59 dimerizes through the downstream coiled-coil rich region (Abdul Kader et al., 2017).
60 Invertebrate genomes do not encode homologous proteins of MTCL1, suggesting
61 that the MT-regulating activities of MTCL1 are specifically utilized in vertebrates. In
62 addition, vertebrate genomes encode a single paralog of MTCL1, which we named
63 MTCL2 (GenBank accession number: NM_001164663). The deduced amino acid
64 sequence showed significant homology with MTCL1 in the central coiled-coil region and
65 the C-MTBD, but not in the N-MTBD (Fig. 1A-C). This suggests that vertebrates exploit
66 another MT-regulating protein with similar but not identical activity to that of MTCL1.

In this study, we aimed to examine whether MTCL2 functions as a homolog of MTCL1, and if so, to dig into the similarities and differences between these MTCLs. The first question is particularly important considering that a mouse MTCL2 isoform lacking the 203 N-terminal amino acids has already been reported as SOGA (suppressor of glucose from autophagy) with completely different functions than those of MTCL1 (Fig. 1A) (Combs and Marliss, 2014; Cowherd et al., 2010). According to the previous paper, SOGA is translated as a membrane-spanning protein and cleaved into two halves in the ER of hepatocytes (Cowherd et al., 2010). The resultant N-terminal fragment is released into the cytoplasm to suppress autophagy by interacting with the Atg12/Atg5 complex, whereas the C-terminal fragment is secreted after further cleavage (see Fig. 1A, boxed illustration). In this context, we first analyzed the expression, subcellular localization, and functions of MTCL2, and concluded that uncleaved MTCL2 works as a novel MT-regulating protein in the cytosol, at least in several cell lines. Our results indicated that MTCL2 associates with the Golgi membrane, where it crosslinks but does not stabilize MTs through the conserved C-MTBD. Knockdown experiments demonstrated that these activities of MTCL2 are required for the accumulation of MTs around the Golgi and the clustering of Golgi stacks into a compact Golgi ribbon. *In vitro* wound healing assays further suggested a possible intriguing activity of MTCL2 in integrating the centrosomal and Golgi-associated MTs around the Golgi ribbon, thus being essential for directional migration. Since MTCL1 and 2 localize on microtubules in a mutually exclusive manner, the present results demonstrate that cells utilize two members of the MTCL protein family to differentially regulate the Golgi-associated MTs for controlling cell polarity.

Results

MTCL2 is expressed predominantly as an 180kDa full-length protein without cleavage

SOGA, a mouse MTCL2 isoform lacking the 203 N-terminal amino acids, is cleaved into several fragments in hepatocytes (see boxed illustration in Fig. 1A) (Cowherd et al., 2010). To examine whether MTCL2 functions as an MTCL1 paralog, we first analyzed the molecular mass of MTCL2 in several cell lines including a human liver cancer cell line, HepG2. Based on epitope position, the commercially available anti-SOGA antibody was predicted to detect an 80kDa N-terminal fragment if MTCL2 was subjected to cleavage as reported previously (Fig. 1A) (Cowherd et al., 2010). As shown in Fig. 1D, V5-tagged mouse MTCL2 exogenously expressed in HEK293T cells was detected as a single major band with a molecular mass of around 180kDa, consistent with the nominal molecular weight of 185,656 predicted from the cDNA sequence of mouse MTCL2 (GenBank accession number: NM_001164663), although very weak signals were observed just below the major band. Anti-V5 antibody also revealed the same staining pattern (data not shown). When the antibody was examined for extracts of HeLa-K, HepG2, and RPE1 cells, bands with a similar molecular mass to V5-mMTCL2 were mainly detected, and they disappeared in cells subjected to MTCL2 knockdown (Fig. 1D). As several minor bands were also absent in knockdown cells, they may represent isoforms or cleaved products of MTCL2, particularly in RPE1 cells. However, most of their molecular masses are larger than 135kDa. Therefore, these data indicate that endogenous MTCL2 in these cells is not subjected to the cleavage previously reported for SOGA.

Western blotting analysis of various mouse tissue extracts also revealed a similar 180kDa band as a major band in the lung, testis, ovary, cerebrum, and cerebellum (Fig.1 E). These results suggest that MTCL2 is expressed as a full-length protein rather ubiquitously. The tissue distribution pattern of MTCL2 is similar to that of MTCL1 (Satake et al., 2017), indicating the possibility that these two MTCL family members work simultaneously.

MTCL2 colocalizes with the perinuclear microtubules and Golgi membrane

Next, we examined the subcellular localization of MTCL2 in HeLa-K cells. The anti-SOGA antibody revealed granular signals accumulating near the perinuclear region (Fig. 2A), which disappeared in MTCL2 knockdown cells (see Fig. 5 and 6). In the perinuclear region, these granular signals were frequently arranged in linear order along MTs (Fig. 2A, enlarged view). Consistently, MTCL2 showed strong colocalization with stabilized perinuclear MTs stained with anti-acetylated tubulin antibody (Fig. 2B, C). However, MTCL2 signal was not significantly observed around dynamic MTs invading the peripheral region (Figs.2A and 3). These results suggest that MTCL2 preferentially associates with Golgi-associated MTs, similar to MTCL1(Sato et al., 2014). In fact, MTCL2 signals partially overlapped with those of the cis-Golgi marker proteins GM130 (Fig. 2C) and GS28 (Fig. 3). Close inspection using super-resolution microscopy further revealed the possibility that MTCL2 mediates the association of the Golgi membrane with stabilized MTs (Fig. 2D, arrows).

To further support the above results, we next examined the subcellular localization of exogenously expressed MTCL2 (Supplementary Fig.1). When highly expressed in HeLa-K cells, exogenous MTCL2 induced thick MT bundles and disrupted the normal

Golgi ribbon structure (Supplementary Fig. 1A, B, arrows). However, when the expression was suppressed to endogenous levels, exogenous MTCL2 mimicked the subcellular localization of endogenous MTCL2, by showing accumulation to one side of the perinuclear region and colocalization with Golgi-associated MTs.

In Fig. 3, we compared the subcellular localization of MTCL2 with MTCL1 and another MT lattice-binding protein MAP4, a classical MAP expressed in HeLa-K cells (Chapin and Bulinski, 1991). MAP4 exhibits a rather continuous distribution on MTs without strong preference for Golgi-associated MTs. In contrast, both MTCL1 and 2 intermittently localize on MTs and are specifically condensed on Golgi-associated MTs. These results indicate that the localization pattern of MTCL2 is indeed a characteristic feature of MTCL protein family members.

MTCL2 associates with MTs and the Golgi membrane independently through the C-terminal and N-terminal regions, respectively

To determine which regions are responsible for the subcellular localizations of MTCL2, we subdivided the molecule into three fragments, N, M, and C, and expressed them as V5-tagged forms to examine their localization in HeLa-K cells (Fig. 4A, B). As expected, the C-terminal fragment of MTCL2 (C), which contained the region corresponding to MTCL1 C-MTBD, colocalized with MTs (Fig. 4B, top panels). Direct binding with MTs was further confirmed using a shorter fragment of MTCL2 (CT1), still containing the putative C-MTBD (Fig 4A and C). CT1 fused with MBP (maltose-binding protein), but not MBP alone, was co-sedimented with MTs *in vitro* when purified from *E. coli* and mixed with taxol-stabilized MTs (Fig. 4C). A smaller C-terminal fragment, which

completely corresponded to the C-MTBD of MTCL1, colocalized with MTs, although it tended to accumulate in the nucleus (Fig.8D). Taken together, these results indicate that MTCL2 directly interacts with MTs through the conserved C-terminal region corresponding to the C-MTBD of MTCL1.

Fig. 4B also indicates that, contrasting to MTCL1 (Fig. 4B, bottom panels), the N-terminal fragment of MTCL2 (N) did not colocalize with MTs when expressed in HeLa-K cells. Instead, this fragment clearly colocalized with the Golgi membrane stained with anti-GM130 antibody. Together with the results that the middle fragment, M, distributed diffusely without showing any discrete localizations (Fig. 4B), these results indicate that MTCL2 associates with MTs and the Golgi membrane independently through the C-terminal and N-terminal regions, respectively. Since the C-terminal fragment did not show preferential binding to the perinuclear MTs (Fig. 4B), these results suggest that preferential association of MTCL2 with the perinuclear, Golgi-associated MTs is the consequence of the dual binding activity of MTCL2 with MTs and the Golgi membrane.

MTCL2 depletion reduced the accumulation of perinuclear MTs and induced lateral expansion of the Golgi ribbon structures

To explore the physiological function of MTCL2, we next analyzed the effects of MTCL2 knockdown in HeLa-K cells. For this purpose, we first established heterogeneous stable cells expressing mouse MTCL2 in a doxycycline-dependent manner (see Materials and Methods). When cells were transfected with control siRNA in the absence of doxycycline (without exogenous MTCL2 expression), many cells showed strong accumulation of MTs around the perinuclear region at which endogenous MTCL2 is

concentrated (Fig. 5A). In contrast, cells subjected to MTCL2 knockdown in the absence of doxycycline exhibited complete loss of MTCL2 signal and severely reduced accumulation of MTs around the perinuclear region (Fig. 5A). The specificity of these knockdown effects was confirmed by a rescue experiment in which doxycycline was added to induce expression of RNAi-resistant MTCL2 (mouse MTCL2) at endogenous levels. Under these conditions, many cells restored MT accumulation in the perinuclear region, where the exogenous MTCL2 is concentrated. Fig. 5B shows the quantitatively analyzed data of these experiments. Here, we estimated the asymmetric distribution of MTs by calculating the skewness of the intensity distribution for tubulin signals within each cell (Fig. 5B, top panel). In control cells, the pixel intensity of tubulin signals was distributed with skewness ~ 0.8 (median), whereas in MTCL2 knockdown cells this value decreased to ~ 0.5, indicating a more symmetric distribution of MTs. Expression of RNAi-resistant mouse MTCL2 restored the value to ~ 0.65, statistically supporting its rescue activity. We further confirmed that expression of an MTCL2 mutant lacking C-MTBD (mMTCL2 ΔC-MTBD) could not restore the perinuclear accumulation of MTs in MTCL2 knockdown cells (Fig. 5C, D). These results suggest that MTCL2 promotes the accumulation of MT through MT binding via C-MTBD.

Interestingly, MTCL2 knockdown also affected the morphology of Golgi ribbons (Fig. 6). Contrasting to control cells, which showed a compact crescent-like morphology of the Golgi ribbon at one side of the nucleus, MTCL2 knockdown cells exhibited abnormally expanded Golgi ribbons along the nucleus (Fig. 6A). The median expansion angle (θ) of the Golgi apparatus (see top panel of Fig. 6B) was 84.3° for control cells, whereas it significantly increased to 106.3° in MTCL2 knockdown cells (Fig. 6B). Again, expression of RNAi-resistant MTCL2 reduced the angle with a median value of 76.6°, indicating that

MTCL2 is essential for compact accumulation of the Golgi ribbon. The MTCL2 ΔC-MTBD mutant failed to rescue this phenotype (Fig. 6C and D). Similar effects of MTCL2 knockdown were observed in RPE1 cells (Supplementary Fig. 3). Altogether, these results demonstrate that MTCL2 plays important roles in the perinuclear accumulation of MTs and the morphology of Golgi ribbons.

MTCL2 depletion resulted in defects in cell migration

Previous studies have demonstrated that the Golgi ribbon structure and its associated MTs are essential for maintaining directed cell migration due to its essential roles in the polarized transport of vesicles (Bergmann et al., 1983; Miller et al., 2009; Rivero et al., 2009; Sato et al., 2014; Yadav et al., 2009). Therefore, we next examined whether MTCL2 depletion affected directed cell migration during *in vitro* wound healing process.

First, HeLa-K cells transfected with control or MTCL2 siRNA were grown to a confluent monolayer and scratched with a micropipette tip to initiate directional migration into the wound. In control cells at the wound edge, reorientation of the Golgi and elongation of a densely aligned MT toward the wound were clearly observed (Fig. 7A). In MTCL2 knockdown cells, reorientation of the Golgi was reduced but not severely affected. Nevertheless, cells lacking MTCL2 exhibited randomly oriented MTs and failed to align them toward the wound (Fig. 7A).

Despite the significant difference in MT organization in cells at the wound edge, we could not estimate the effects of MTCL2 knockdown on directional migration because HeLa-K cells migrated very slowly. Thus, we used RPE1 cells to estimate wound healing velocity, and found that cells lacking MTCL2 migrated significantly slower than control

234 cells (Fig. 7B, Supplementary Movies 1 and 2). By comparing the normalized areas newly
235 covered by migrated cells, the directed migration velocity of MTCL2 knockdown cells
236 was estimated to be ~50% of that of control cells (Fig. 7B). Time-lapse analysis of
237 differential interference contrast (DIC) images indicated that cells lacking MTCL2
238 exhibited abnormally elongated shapes and showed less efficiency in extending
239 lamellipodia (Supplementary Movie 2). Reorientation of the Golgi position toward the
240 wound was observed in MTCL2 knockdown cells to a similar extent as control cells (Fig.
241 7C, D). In addition, in contrast to HeLa-K cells, polarized elongation of MTs toward the
242 wound was also observed, even in MTCL2 knockdown cells (Fig. 7C). However, the
243 proximal ends of these MTs looked rather unfocused. Close inspection demonstrated that
244 in MTCL2 knockdown cells at the wound edge the Golgi ribbon was frequently separated
245 from the centrosome and sometimes detached from the nucleus (Fig. 7 C and E). As a
246 result, the centrosomal MTs and Golgi-associated MTs elongated from different positions
247 towards the wound, and could be clearly discerned in many MTCL2 knockdown cells.
248 This was in sharp contrast to control cells, in which the centrosome and Golgi-ribbon
249 were tightly linked near the nucleus and the proximal part of the centrosomal and Golgi-
250 associated MTs were focused together indistinguishably. These results suggest an
251 intriguing possibility that MTCL2 plays an essential role in integrating the centrosomal
252 and Golgi-associated MTs by crosslinking them on the Golgi membrane.
253
254 **Relationship between MTCL2 and MTCL1**
255
256 Finally, we examined the relationship between MTCL1 and MTCL2 with respect to
257 their localization and function. To compare their localization, we analyzed HeLa-K cells

stably expressing V5-tagged MTCL2 at a level comparable to that of the endogenous one (Fig. 8A). Triple staining of the cells with anti-V5, anti-MTCL1, anti-α-tubulin antibodies revealed that granular signals of MTCL1 and 2 hardly overlapped even when both of them were on MTs. These results indicate that MTCL1 and 2 interact with MTs in a mutually exclusive manner. Next, we examined the interaction between endogenous MTCL1 and 2 in HeLa-K cells, since these coiled-coil proteins were shown to form a heterogeneous complex when simultaneously overexpressed in HEK293T cells (data not shown). In Fig. 8B, we immunoprecipitated endogenous MTCL1 from HeLa-K cells and examined the presence of MTCL2 in the immunocomplex. Although the experiment was performed to precipitate whole MTCL1 in the input (data not shown), less than 10% of MTCL2 in the input was condensed in the immunocomplex. This indicates that a substantial fraction of MTCL2 exists without forming a heterooligomer with MTCL1. These results are consistent with the immunostaining results in Fig. 8A, and indicate that MTCL1 and 2 exist independently in the same cells. We also confirmed that MTCL2 knockdown did not affect the perinuclear localization of MTCL1, supporting that both proteins localize independently on Golgi-associated MTs.

In a previous study, we demonstrated that MTCL1 knockdown does not affect MT organization significantly, but specifically reduces anti-acetylated tubulin signal on the perinuclear MTs (Sato et al., 2014). This is in sharp contrast to the present results that MTCL2 knockdown markedly affected MT organization (Fig. 5A), but did not significantly reduce tubulin acetylation signals (Fig. 8C). These results suggest the possibility that the C-MTBD of MTCL2 lacks MT stabilization activity due to the sequence diversity of MTCL1 CMTB (red line in Fig. 1C). To examine this possibility, we expressed GFP-CMTB of MTCL1 and 2 in HeLa-K cells, and analyzed their effects

on tubulin acetylation, as a marker of MT stabilization (Fig. 8D). As previously demonstrated, GFP-MTCL1 C-MTBD strongly induced tubulin acetylation in the MTs to which it associated even at low concentration (Abdul Kader et al., 2017). However, the association of GFP-MTCL2 C-MTBD with MTs did not induce tubulin acetylation even at higher concentrations. Noteworthy, the CMTB of MTCL1, but not MTCL2 caused MT bundling, which is considered a secondary effect of MT stabilization (also see Fig. 4B). We confirmed these results quantitatively by western blotting analysis of HEK293T cell extracts expressing each CMTB construct (Fig. 8E) (Sato et al., 2014). The results clearly indicate that expression of MTCL1 C-MTBD but not MTCL2 C-MTBD dramatically increased tubulin acetylation. Taken together, these results demonstrate that MTCL1 and 2 independently localized to the Golgi-associated MTs and exert distinct MT-regulating functions to differentially contribute to the development of cell polarity.

Discussion

In the present study, we demonstrate that MTCL2, the mammalian MTCL1 paralog, is a novel MT-regulating protein that preferentially localizes to the Golgi membrane and plays essential roles in perinuclear MT accumulation and Golgi ribbon morphology.

A shorter variant of MTCL2 was reported in 2010 and named SOGA (Cowherd et al., 2010), the putative internal signal sequence of which was hypothesized to direct its translation and cleavage in ER. The present data indicate that, albeit containing whole SOGA sequences, MTCL2 is mainly expressed in a full-length form without cleavage and functions in the cytosol as an MT-regulating protein. We cannot completely exclude the possibility that a minor fraction of MTCL2 is processed in cultured cells as previously predicted. Alternatively, this process could occur predominantly in the liver to function as a suppressor of glucose by autophagy (SOGA). However, the results presented here are highly consistent with the notion that this gene product dominantly functions as an MT-regulating protein, but not as a SOGA. Based on these results, we propose that this gene product should be called MTCL2 instead of SOGA. This conclusion is supported by a recent study that identified SOGA as a CLASP2-binding protein by mass spectrometry (Kruse et al., 2017). This conclusion is also supported by our observation that MTCL2 knockdown did not induce LC3-positive autophagosomes in HepG2 cells (Supplementary Fig. 3). In addition, we have to mention that we failed to confirm the presence of the putative internal signal sequence as well as Atg16- and Rab5-binding motifs in the MTCL2 sequence, all of which were discussed in a previous paper (see Fig. 1A, boxed illustration) (Cowherd et al., 2010).

Consistent with the overall homology with MTCL1, MTCL2 exhibits several similar

319 features of MTCL1. It shows homo-oligomerization activity via the coiled-coil region
320 (Supplementary Fig. 4), localizes to the Golgi membrane, and interacts with MTs through
321 the C-terminal region. We also demonstrated that, similar to MTCL1, MTCL2
322 knockdown in RPE1 cells impaired directional migration without significantly affecting
323 the Golgi repolarization (Sato et al., 2014). On the other hand, we noticed that MTCL2
324 has characteristic features distinct from those of MTCL1. The most striking difference is
325 that MTCL2 only has a single MT-binding region in the C-terminus, and this C-MTBD
326 lacks the MT-stabilizing activity observed for MTCL1 C-MTBD. This indicates that the
327 major role of MTCL2 is to crosslink and accumulate MTs on the Golgi membrane (Fig.
328 9A and B). MTCL1 was named after its MT crosslinking activity via N-MTBD (Sato et
329 al., 2013). However, accumulating data demonstrated that the MT-stabilization activity of
330 C-MTBD is essential for its physiological roles (Satake et al., 2017). In addition, in
331 cultured cells, we demonstrated that the MT stabilization activity of MTCL1 is
332 fundamentally required for the stable development of the Golgi-nucleated MTs, which
333 are subsequently crosslinked by N-MTBD (Fig. 9B) (Sato et al., 2014). Therefore,
334 together with the present results that MTCL1 and 2 associate with MTs in a mutually
335 exclusive manner without forming a heterocomplex, these results suggest that these two
336 members of the MTCL family exert distinct roles for MT organization on the Golgi
337 membrane. MTCL1 mainly supports the development of Golgi-nucleated MTs by
338 stabilizing their elongation, whereas MTCL2 crosslinks and accumulates these MTs
339 around the Golgi (Fig. 9B).

340 Interestingly, in RPE1 cells at the wound edge, MTCL2 knockdown led to the
341 separation of the centrosome and Golgi ribbon. In these cells, MTs emanating from the
342 centrosome and those associated with the Golgi were clearly distinct, although both of

343 them independently invaded lammellipodia. These results are consistent with a previous
344 work demonstrating that disconnecting the Golgi ribbon from the centrosome prevents
345 directional migration (Hurtado et al., 2011), and raise the intriguing possibility that the
346 MT crosslinking activity of MTCL2 plays an important role in integrating centrosomal
347 and Golgi-associated MTs. To establish directional cell migration, repolarization of the
348 Golgi to the wound (Etienne-Manneville and Hall, 2001; Kupfer et al., 1982) and
349 development of the Golgi ribbon structure (Miller et al., 2009; Rivero et al., 2009) have
350 been shown to be required. The present results proposed that the integration of
351 centrosomal and Golgi-associated MTs represents the third requirement for directional
352 migration. MTCL2 knockdown-dependent separation of the centrosome and the Golgi
353 ribbon was not clearly observed in HeLa-K cells, which did not show active migration.
354 Therefore, the integration of centrosomal and Golgi-derived MTs by MTCL2 might be
355 particularly important for actively migrating cells, in which MTs must be subjected to
356 various mechanical stresses (Etienne-Manneville, 2013).

357 In addition to the effects on MTs, MTCL2 knockdown caused expansion of the
358 crescent-like morphology of the Golgi ribbon along the nucleus. Since RNAi-resistant
359 MTCL2 mutant lacking the C-MTBD (MTCL2 ΔC-MTBD) did not rescue this phenotype,
360 crosslinking and accumulation of the Golgi-associated MTs by MTCL2 may indirectly
361 facilitate the clustering of the Golgi ribbon (Fig. 9A). However, at present, we cannot
362 conclusively propose this model as MTCL2 ΔC-MTBD failed to localize to the Golgi and
363 diffusely distributed in the cytosol. This means that loss of C-MTBD leads to the loss of
364 Golgi association activity, and raises the possibility that the lack of rescue activity of
365 MTCL2 ΔC-MTBD might be due to the lack of Golgi-binding activity, but not due to the
366 lack of the MT-binding activity. Our deletion mutant analysis (Fig. 4) clearly indicated

that the N-terminal region was sufficient for the Golgi association. Therefore, loss of the Golgi association activity in MTCL2 ΔC-MTBD was unexpected. One possible explanation is that the Golgi association activity of MTCL2 is masked in the full-length molecule by, for example, an intramolecular interaction, and MT binding through the C-MTBD releases the inhibition. Examination of this model as well as identification of the target molecule of MTCL2 for its Golgi localization (X in Fig. 9B) are important directions for our future study.

Materials and methods

Molecular biology

The cDNA clone encoding full-length mouse MTCL2 (GenBank accession number: AK147227) was purchased from Danaform (Kanagawa, Japan). After confirming sequence identity with NM_001164663, a DNA fragment corresponding to the MTCL2 open reading frame was subcloned into an expression vector, pCAGGS-V5. Subsequently, several deletion mutants of MTCL2 were constructed in pCAGGS-V5, pEGFP-c2 (Takara Bio Inc., Japan), or pMal-c5x (New England Biolabs). To establish heterogeneous stable transformants, mouse MTCL2 and its mutants with or without a 6 × V5-tag were subcloned in pOSTet15.1 (kindly provided by Y. Miwa, University of Tsukuba, Japan), an Epstein–Barr virus (EBV)-based extrachromosomal vectors carrying a replication origin (oriP) and replication initiation factor (EBNA-1) sufficient for autonomous replication in human cells (Tanaka et al., 1999). Human and mouse MTCL1 cDNA (GenBank accession numbers: AB018345 and AK147691, respectively) used were described previously (Sato et al., 2013).

Antibodies

Anti-KIAA0802 pAb (W19) (Santa Cruz Biotechnology) and anti-SOGA1 polyclonal antibody (pAb) (HPA043992) (Sigma-Aldrich) were used to detect MTCL1 and MTCL2, respectively. To detect other proteins, the following antibodies were used: anti-α-tubulin monoclonal Ab (mAb) (DM1A), anti-acetylated tubulin mAb (6-11B-1), anti-MAP4 mAb (H-300), and anti-GFP mAb (B-2) (Santa Cruz Biotechnology); anti-V5 mAb (R960-25) (Thermo Fisher); anti-GM130 mAb (35/GM130), anti-GS28 (1/GS28) (BD

Transduction Laboratories); anti-GAPDH mAb (6C5) (Hytest ltd.); anti-β-tubulin (KMX-1) (Upstate/Millipore); anti-pericentrin pAb (ab4448) (Abcam); LC3 mAb (M152-3) (MBL, Japan).

Cell culture and plasmid transfection

HeLa-Kyoto (HeLa-K), HEK293T, and HepG2 cells were cultured in Dulbecco's modified Eagle's medium (low glucose) (Nissui, Japan) containing 10% fetal bovine serum, 100 U/mL penicillin, 100 μg/mL streptomycin, and 1 mM glutamine at 37°C in 5% CO_2. Immortalized human pigment epithelial cells, hTERT-RPE1 (RPE1) cells were maintained in a 1:1 mixture of DMEM/Ham's F12 (FUJIFILM WAKO Pure Chemical Corporation, Japan) containing 10% fetal bovine serum, 100 U/mL penicillin, 100 μg/mL streptomycin, 10 μg/mL hygromycin B, and 1 mM glutamine at 37°C in 5% CO2. When subjected to immunofluorescent analysis, cells were seeded on coverslips settled down in 24-well plates and coated with atelocollagen (0.5 mg/mL IPC-50; KOKEN, Japan). Plasmid transfections were performed using polyethyleneimine (Polysciences, Inc.) for HEK293T cells or Lipofectamine LTX (Life Technologies Corporation) for HeLa-K cells according to the manufacturer' s instructions. To establish heterogenous stable HeLa-K cells expressing mouse MTCL2 in a doxycycline-dependent manner, cells were transfected with pOSTet15.1 expression vector encoding the appropriate MTCL2 cDNA. The following day, cells were reseeded at one-twentieth of the cell density, and subjected to selection using medium containing 800 μg/mL G418 disulfate (Nacalai Tesque, Japan) for more than 6 days. The surviving cells were used in the following experiments without cloning.

423

424 **RNAi experiments and wound healing assays**

425

426 The siRNA oligonucleotide sequences used for MTCL2 knockdown in human cultured
427 cells were as follows: #2: 5'-GAGCGACCGAGAGAGCAUUCC-3' and #5:
428 CUGAAGUACCGCUCGCUCUdTdT. As control, a non-silencing RNAi
429 oligonucleotide (All stars negative control siRNA: Qiagen) was used. Cells were seeded
430 on coverslips at densities of 1.2 ~ 4 × 10^4 cells, and transfected with siRNA
431 oligonucleotide at final concentrations of 10 – 17 nM using RNAiMax (Life Technologies
432 Corporation) according to the manufacturer' s instructions. siRNA transfection was
433 repeated the day after medium change, and cells were subjected to immunofluorescence
434 analysis on day 3. For rescue experiments, heterogeneous stable HeLa-K cells expressing
435 mouse MTCL2 were subjected to a similar protocol, except that 100 ng/mL of
436 doxycycline was always included in the medium after the 1st siRNA transfection. For
437 wound healing analysis, HeLa-K cells subjected to RNAi were scratched with a
438 micropipette tip on day 4. RPE1 cells were seeded at 5 × 10^4 cells in one compartment of
439 35 mm glass bottom culture dish separated into 4 compartments (Greiner, 627870) after
440 coating with 10 μg/mL fibronectin (FUJIFILM, Japan, 063-05591), and siRNA
441 transfections were performed as described above. Wounds were made on day 4 by
442 scratching cell monolayers with a micropipette tip and subjected to live imaging.

443

444 **Cell extraction and western blotting**

445

446 Cell extracts were prepared by adding RIPA buffer (25mM Tris/HCl pH 7.5, 150mM

NaCl, 1% NP40, 1% deoxycholic acid, 0.1% SDS) containing protease inhibitor cocktail (Sigma, P8340) followed by brief sonication and centrifugation (15,000 × g, 15 min). For tissue distribution analysis of MTCL2, the mouse tissue lysates prepared in a previous study were used (Satake et al., 2017). Samples were separated by SDS-PAGE and then transferred to polyvinyldifluoride membranes. Blots were incubated in blocking buffer containing 5% (w/v) dried skim milk in PBST (8.1mM Na2HPO4.12H2O, 1.47mM KH2PO4, 137mM NaCl, 2.7mM KCl, and 0.05% Tween 20) followed by overnight incubation with the appropriate antibodies diluted in blocking buffer. Dilutions of anti-SOGA pAb and anti-GAPDH mAb were 1:1000 and 1:5000, respectively. Secondary antibodies were diluted to 1:2,000. Blots were then exposed to horseradish peroxidase (HRP)-conjugated secondary antibodies (GE Healthcare) diluted in blocking buffer for 60 min at RT and washed again. Blots were visualized using Immobilon Western Chemiluminescent HRP Substrate (Millipore) or ECL western blotting detection system (GE Healthcare), and chemiluminescence was quantified using the ImageQuant LAS4000 Luminescent Image Analyzer (GE Healthcare).

Immunofluorescence staining

Cells were fixed with cold methanol for 10 min at −20°C, followed by blocking with 10% (v/v) fetal bovine serum in PBST. To visualize the Golgi localization of exogenous MTCL2, cells were treated with modified PBST containing 0.5% TritonX-100 instead of Tween20 for 10 min after fixation. Samples were then incubated with appropriate primary antibodies diluted in TBST (10mM Tris–HCl, pH 7.5, 150mM NaCl, 0.01% (v/v) Tween 20) containing 0.1% (w/v) BSA for 45 min at RT, except for MTCL1 and 2 staining,

471 which were performed overnight at 4ºC. After washing with PBST, samples were
472 visualized with the appropriate secondary antibodies conjugated with Alexa Fluor 488,
473 555, or 647 (Life Technologies Corporation) by incubating for 45min at RT. Antibodies
474 were diluted as follows: anti-KIAA0802 pAb (1/1000), anti-SOGA pAb (1/2000), anti-α-
475 tubulin mAb (1:1,000), anti-acetylated tubulin mAb (1:1,000), anti-V5 mAb (1:4,000),
476 anti-GM130 mAb (1:1,000), anti-GS28 mAb (1:300), anti-GFP mAb (1:2,000), anti-
477 MAP4 mAb (1:1000), anti-β-tubulin (1:2000), anti-pericentrin pAb (1:1000), and anti-
478 LC3 mAb (1:300). All secondary antibodies were used at a 1:2000 dilution. The nuclei
479 were counterstained with DAPI (4', 6-diamidino-2-phenylindole) (MBL, Japan) at a
480 1:2000 dilution in PBST during the final wash. For image acquisition, samples on
481 coverslips were mounted onto glass slides in Prolong Diamond Antifade Mountant
482 (Thermo Fisher).
483
484 **Image acquisition and processing**
485
486 High-resolution images were acquired using a Leica SP8 laser scanning confocal
487 microscopy system equipped with an HC PL APO 63x/1.40 Oil 2 objective, using the
488 Hybrid Detector in photon counting mode. To obtain super-resolution images,
489 HyVolution2 imaging was performed on the same system using Huygens Essential
490 software (Scientific Volume Imaging) (Borlinghaus and Kappel, 2016). To obtain wide
491 view images for quantification (for Figs. 5 and 6), conventional fluorescence images were
492 obtained using an AxioImager ZI microscope (Carl Zeiss, Oberkochen, Germany)
493 equipped with a Plan APCHROMAT 40×/0.95 objective using Orca II CCD camera
494 (Hamamatsu Photonics, Shizuoka, Japan). The laterally expanding angle of the Golgi

apparatus around nuclei and skewness of pixel intensity were quantified using the "Measure" function of ImageJ software. For statistical analysis, photographs of several fields containing ~40 cells with similar density were taken from two independent experiments, and all cells in each field were subjected to quantification analysis to avoid selection bias. In rescue experiments, ~100 cells expressing exogenous MTCL2 at similar expression levels as endogenous one were collected from ~10 fields with similar cell densities. For live cell imaging, differential interference contrast (DIC) images were acquired using a Leica SP8 confocal microscopy system equipped with an HCX PL APO 10x/0.40 objective using a 488nm laser line. Areas newly covered by migrated cells during wound healing for 440min were estimated using the "Measure" function of ImageJ software and normalized by the length of the corresponding wound edge at time 0.

MT-binding assay

MBP (maltose binding protein) or MBP-mMTCL1 CT1 were purified from the soluble fraction of *E. coli* according to the standard protocol, and dialyzed against BRB buffer (80 mM PIPES-KOH pH 6.8, 1 mM $MgCl_2$, 1 mM EGTA). Each MBP protein was incubated with taxol-stabilized MTs (both final concentrations of the sample protein and α/β-tubulin heterodimer were 0.5 mg/mL) in BRB supplemented with 1.5 mM $MgCl_2$ and 1mM GTP for 15 min at RT, and subjected to centrifugation (200,000 × g) for 20 min at 25°C on a cushion of 40% glycerol in BRB buffer. After carefully removing the supernatant and glycerol cushion, the resultant MT pellet was gently washed with PBST 3 times and solubilized with SDS sample buffer (10% β-mercaptoethanol, 125 mM Tris-HCl, pH 6.8, 2% SDS, 10% glycerol, and 0.005% bromophenol blue) for subsequent

519 SDS-PAGE analysis.

520

521 **Immunoprecipitation and pull-down experiments**

522

523 HeLa-K cells (~ 5×10^6 cells) were solubilized in 1mL lysis buffer (20mM Tris-HCl, pH
524 7.5, 150mM NaCl, 1% NP-40, 1mM DTT) containing a cocktail of protease and
525 phosphatase inhibitors (Roche Applied Science) for 30 min at 4°C, briefly sonicated, and
526 centrifuged at 15,000 × g for 30 min. The resulting supernatants were mixed with
527 Dynabeads Protein G (Thermo Fisher) conjugated with 2μg of anti-MTCL1 antibody for
528 ~ 2 h at 4°C. Immunoprecipitates were boiled in SDS sample buffer and subjected to
529 western blot analysis. In pull-down experiments, HEK293T cells were transfected with
530 appropriate expression vectors and subjected to the same procedure as described above,
531 except that streptavidin-conjugated Sepharose (GE Healthcare) was used instead of
532 Dynabeads.

533

534

Acknowledgement

The authors thank Yoshihiro Miwa (University of Tsukuba) for providing the pOSTet15.1 expression vector gift. We would like to thank Editage (www.editage.com) for English language editing. This work was supported by KAKENHI (to A.S.) (Grant Numbers 16H04765 and 19H03228) of the Ministry of Education, Culture, Sports, Science and Technology (MEXT) of Japan.

Author contributions

A.S. planned and performed the experiments, interpreted the results, and wrote the paper. R.M., M.M, S.M, and Y.I. performed the experiments.

Conflict of interest

The authors declare no competing financial interests.

552 **Figure legends**

553

554 **Figure 1. MTCL2 is expressed predominantly as an 180kDa full-length protein**
555 **without cleavage.** (A) Predicted molecular structure of mouse MTCL2 (mMTCL2) and
556 its amino acid sequence homology with mouse MTCL1 (mMTCL1). CC (dark blue)
557 indicates the region with highest score (> 0.85) of coiled-coil prediction, whereas CCL
558 (light blue) indicates the region with moderate score (>0.4) (https://embnet.vital-
559 it.ch/software/COILS_form.html). A black bar labeled 'epitope' indicates the position of
560 the antigen peptide against which the used antibody was generated (commercially
561 available anti-SOGA antibody). The boxed illustrations in the bottom indicate the position
562 of mouse SOGA (mSOGA) in comparison with mMTCL2, and summarize the arguments
563 in the paper reporting SOGA (Cowherd et al., 2010). Green bar indicates the predicated
564 position of the internal signal sequence, whereas green dotted arrows indicate the
565 predicted positions of cleavages. We failed to confirm all arguments indicated here by
566 ourselves. (B, C) Sequence alignment of the N and C-terminal region of mouse MTCL1
567 and 2. The MTCL1 sequence surrounded by bold line corresponds to the N- and C-MTBD
568 (B and C, respectively). Red line in C indicates the region where MTCL2 sequence
569 significantly diverges from that of MTCL1 C-MTBD. (D) Western blotting analysis to
570 estimate the molecular mass of MTCL2 expressed in various cultured cells. In lane 1~3,
571 cell extracts of HEK293T expressing exogenously expressed V5-mMTCL2 were loaded
572 after indicated dilution. In other lanes, extracts of indicated culture cells with or without
573 MTCL2 knockdown were loaded. NS: non-silencing control. #2 and #5 indicate different
574 siRNA oligonucleotides for MTCL2. (E) Tissue distribution of MTCL2. Total extracts
575 from the indicated mouse tissues (25μg/lane) were loaded for western blotting analysis
576 using anti-SOGA antibody. In lane 1, total cell extracts of HEK293T expressing

577 exogenously expressed V5-mMTCL2 were loaded as a positive control.

578

579 **Figure 2. MTCL2 specifically colocalizes with stable perinuclear microtubules.** (A-
580 C) HeLa-K cells were stained with anti-SOGA (MTCL2) together with anti-α-tubulin (A),
581 anti-acetylated tubulin (anti-Ac-tub) (B) or anti-GM130 antibody (C). Note that the
582 granular signal of MTCL2 specifically concentrates on the perinuclear MTs but not on
583 the peripheral MTs, and partially co-localizes with GM130. Scale bars, 10μm. (D) HeLa-
584 K cells were triply stained with anti-SOGA, anti-GM130, and anti-acetylated tubulin as
585 indicated. Shown are super-resolution microscopic images. Scale bars, 5μm and 2μm
586 (enlarged panels).

587

588 **Figure 3. Preferential localization to the Golgi-associated MTs is the specific feature**
589 **of MTCL protein family members.** HeLa-K cells were subjected to immunofluorescent
590 analysis using anti-MTCL1, MTCL2 (SOGA), or MAP4 antibodies together with anti-α-
591 tubulin and anti-GS28 (Golgi protein) antibody. At the bottom, similar staining data using
592 anti-acetylated tubulin antibody are shown for comparison. Bars, 20μm and 5μm (insets).

593

594 **Figure 4. MTCL2 associates with MTs and the Golgi membrane independently.** (A)
595 MTCL2 deletion mutants used in this study. (B) Subcellular localization of V5-tagged
596 deletion mutants of mouse MTCL2 in HeLa-K cells. Cells were triply stained with anti-
597 V5, anti-β-tubulin, and anti-GM130 antibodies. In the bottom panel, data of cells
598 expressing V5-mMTCL1 N-terminal fragment (1-916) were shown for comparison. Scale
599 bar, 20μm. (C) The C-terminal fragment of mMTCL2 directly binds to MTs. MBP-fused
600 mMTCL2 CT1 purified from *E.coli.* was examined for MT pull-down experiments. MBP-

mMTCL2 CT1 but not MBP was found to be specifically precipitated only when taxol-stabilized MTs were included.

Figure 5. MTCL2 depletion reduces the perinuclear accumulation of MTs in a C-MTBD dependent manner. (A) HeLa-K cells stably harboring pOSTet15.1 expression vector for mouse MTCL2 were transfected with siRNA oligonucleotides for control or MTCL2 knockdown (#2) in the presence or absence of 100nM doxycycline, and doubly stained with anti-SOGA (MTCL2) and anti-α-tubulin antibody, as indicated on the left. Note that cells subjected to control RNAi show MT accumulations at the perinuclear region where MTCL2 concentrated in the absence of doxycycline (without exogenous expression of mouse MTCL2). Such accumulation of MTs disappeared in MTCL2 knockdown cells (-dox), whereas exogenous expression of RNAi-resistant MTCL2 (+dox) strongly restore the accumulation. Bar: 20μm. (B) Extent of MT accumulation was quantitatively estimated by calculating the skewness of the pixel intensity distribution for tubulin fluorescence signal in each cell. Top panel shows typical data on the distribution, indicating that the asymmetries of tubulin signal distribution are compromised in MTCL2 knockdown cells. Bottom is box plot combined with beeswarm plot of the skewness distribution in each condition. The lines within each box represent medians. Data represent the results of the indicated number (n) of cells from two independent experiments. ** $p<0.01$, estimated by the Wilcoxon test. NS: no significant difference. (C) HeLa-K cells stably harboring pOSTet15.1 expression vector for mouse MTCL2 ΔC-MTBD were subjected to the same experimental procedure as in (A). Note that MT accumulation was not restored by expression of mouse MTCL2 ΔC-MTBD. Bar: 20μm. (D) MT accumulation data in (C) was quantitatively analyzed as in (B). Data

represent the results of the indicated number (n) of cells from two independent experiments. ** $p<0.01$, estimated by the Wilcoxon test.

Figure 6. MTCL2 depletion significantly expands the Golgi ribbon structures. (A) HeLa-K cells stably harboring pOSTet15.1 expression vector for mouse MTCL2 were transected with siRNA oligonucleotide for control or MTCL2 knockdown (#2) in the presence or absence of 100nM doxycycline, and doubly stained with anti-SOGA (MTCL2) and anti-GM130 antibodies, as indicated on the left. Note that cells subjected to control RNAi show compact Golgi ribbon structures at one side of the perinuclear region. Such Golgi ribbon structures become laterally expanded around the nucleus in MTCL2 knockdown cells (-dox), whereas exogenous expression of RNAi-resistant MTCL2 (+dox) strongly restore their compactness. Bar: 20 μm. (B) Quantification of Golgi ribbon expanding angle (θ) around the nuclei (top panel) in each condition. Data represent the results of the indicated number (n) of cells from two independent experiments. ** $p<0.01$, estimated by the Wilcoxon test. NS: no significant difference. (C) HeLa-K cells stably harboring pOSTet15.1 expression vector for mouse MTCL2 ΔC-MTBD were subjected to the same experimental procedure as in (A). Note that compactness of Golgi ribbon was not restored by expression of mouse MTCL2 ΔC-MTBD. Bar: 20 μm. (D) Quantitative analysis as in (B). Data represent the results of the indicated number (n) of cells from two independent experiments. ** $p<0.01$, estimated by the Wilcoxon test.

Figure 7. MTCL2 depletion results in defective cell migration. (A) Confluent monolayers of HeLa-K cells subjected to control or MTCL2 RNAi were fixed and stained

649 with the indicated antibodies 6h after wounding. Cells facing the wound edges (white
650 dotted lines) are shown. Bars, 50 μm. Note that MTCL2-depleted cells did not polarize
651 MT arrays toward the wound. Right panel indicates the percentage of wound-edge cells
652 with correctly oriented Golgi, defined as those falling in the indicated quadrant (white
653 line) in relation to the wound edge. Data represent the means ± S.D. for the indicated
654 number (n) of cells from two independent experiments. NS: no significant difference
655 estimated by the Student's t-test assuming the two-tailed distribution and two-sample
656 unequal variance. (B) Differential interference contrast (DIC) images of wound healing
657 RPE1 cells at 0 min and 7h 20 min after wounding. White dotted line delineated the
658 wound edges. Bars: 200 μm. Right panel indicates quantified data on the areas newly
659 buried by cells after wounding. Data represent the mean ± S.D. of 44 fields taken from
660 two independent experiments. **$p<0.01$, estimated by the Student's t-test assuming the
661 two-tailed distribution and two-sample unequal variance. (C) RPE1 cells subjected
662 wound healing analysis in (B) were fixed and stained with the indicated antibodies. Cells
663 facing the wound edges are shown. Right panels are enlarged view. Note that MTCL2-
664 depleted cells exhibit the separation of the centrosome (white arrowheads) and Golgi,
665 from which MTs are emanating rather independently. Sometimes the centrosome shows
666 significant detachment from the perinuclear region (yellow arrowhead). Bars, 50 μm and
667 20μm (enlarged right panels). (D) Golgi orientation was quantified for wound healing
668 RPE1 cells as indicated in (A). Data represent the means ± S.D. for the indicated number
669 (n) of cells from two independent experiments. NS: no significant difference estimated
670 by the Student's t-test assuming the two-tailed distribution and two-sample unequal
671 variance. (E) Percentage of wound-edge cells with Golgi detached from the centrosome.
672 Data represent the means ± S.D. for the indicated number (n) of cells from two

673 independent experiments. **p<0.01, estimated by the Student's t-test assuming the two-
674 tailed distribution and two-sample unequal variance.
675
676 **Figure 8. MTCL1 and 2 differentially regulate Golgi-associated MTs.** (A) MTCL1
677 and 2 localize on MTs in a mutually exclusive manner. HeLa-K cells stably harboring
678 expression vector for V5-tagged mouse MTCL2 were cultured in the presence of
679 100ng/mL doxycycline, and stained with the indicated antibodies. Shown are super-
680 resolution microscopic images. Scale bars, 5μm and 1μm (enlarged panels). (B) HeLa-K
681 cells transfected with control or MTCL1 siRNA oligonucleotide were subjected to
682 immunoprecipitation with anti-MTCL1 antibody. (C) HeLa-K cells transfected with
683 control or MTCL2 siRNA oligonucleotide were fixed and stained with the indicated
684 antibodies. Bar, 10μm. (D) HeLa-K cells exogenously expressing GFP, GFP-human
685 MTCL1 C-MTBD, or GFP-mouse MTCL2 C-MTBD were immunostained with the
686 indicated antibodies. Bar, 20μm. (E) Total cells extracts of HEK293 cells exogenously
687 expressing GFP, GFP-human MTCL1 C-MTBD, or GFP-mouse MTCL2 C-MTBD were
688 subjected to western blotting analysis using the indicated antibodies.
689
690 **Figure 9. Model for the mechanisms by which MTCL2 regulates Golgi-associated**
691 **MTs, Golgi ribbon morphology, and cell polarity.** (A) MTCL2 parallel dimers
692 crosslink and accumulate MTs on the Golgi membrane, and thereby facilitate the
693 clustering of Golgi stacks into a compact Golgi ribbon. (B) MTCL1 mainly supports the
694 development of the Golgi-nucleated MTs by stabilizing their elongation, whereas MTCL2
695 crosslinks and accumulates MTs around the Golgi and facilitate lateral clustering of Golgi
696 stacks. The present results further indicate a possibility that MTCL2 crosslinks the Golgi-

697 associated MTs with the centrosomal MTs, and thereby integrate these two subsets of MT
698 populations (not illustrated here). X indicates putative target of MTCL2 mediating its
699 Golgi association.

References

Abdul Kader, M., Satake, T., Yoshida, M., Hayashi, I. and Suzuki, A. (2017). Molecular basis of the microtubule-regulating activity of microtubule crosslinking factor 1. *PLoS One* **12**, e0182641.

Akhmanova, A. and Hoogenraad, C. C. (2015). Microtubule minus-end-targeting proteins. *Curr. Biol.* **25**, R162–R171.

Baas, P. W., Rao, A. N., Matamoros, A. J. and Leo, L. (2016). Stability properties of neuronal microtubules. *Cytoskeleton* **73**, 442–460.

Bacallao, R., Antony, C., Dotti, C., Karsenti, E., Stelzer, E. H. K. and Simons, K. (1989). The subcellular organization of Madin-Darby canine kidney cells during the formation of a polarized epithelium. *J. Cell Biol.* **109**, 2817–2832.

Bartolini, F. and Gundersen, G. G. (2006). Generation of noncentrosomal microtubule arrays. *J. Cell Sci.* **119**, 4155–63.

Bergmann, J. E., Kupfer, A. and Singer, S. J. (1983). Membrane insertion at the leading edge of motile fibroblasts. *Proc. Natl. Acad. Sci. U. S. A.* **80**, 1367–1371.

Borlinghaus, R. T. and Kappel, C. (2016). HyVolution—the smart path to confocal super-resolution. *Nat. Methods* **13**, i–iii.

Chabin-Brion, K., Marceiller, J., Perez, F., Settegrana, C., Drechou, A., Durand, G. and Poüs, C. (2001). The Golgi complex is a microtubule-organizing organelle. *Mol. Biol. Cell* **12**, 2047–60.

Chapin, S. J. and Bulinski, J. C. (1991). Non-neuronal 210 x 10(3) Mr microtubule-associated protein (MAP4) contains a domain homologous to the microtubule-binding domains of neuronal MAP2 and tau. *J. Cell Sci.* **98 (Pt 1)**, 27–36.

Combs, T. P. and Marliss, E. B. (2014). Adiponectin signaling in the liver. *Rev. Endocr. Metab. Disord.* **15**, 137–147.

724 **Conduit, P. T., Wainman, A. and Raff, J. W.** (2015). Centrosome function and assembly in animal
725 cells. *Nat. Rev. Mol. Cell Biol.* **16**, 611–624.
726 **Cowherd, R. B., Asmar, M. M., Alderman, J. M., Alderman, E. a, Garland, A. L., Busby, W. H.,**
727 **Bodnar, W. M., Rusyn, I., Medoff, B. D., Tisch, R., et al.** (2010). Adiponectin lowers glucose
728 production by increasing SOGA. *Am. J. Pathol.* **177**, 1936–1945.
729 **Efimov, A., Kharitonov, A., Efimova, N., Loncarek, J., Miller, P. M., Andreyeva, N., Gleeson, P.,**
730 **Galjart, N., Maia, A. R. R., McLeod, I. X., et al.** (2007). Asymmetric CLASP-Dependent
731 Nucleation of Noncentrosomal Microtubules at the trans-Golgi Network. *Dev. Cell* **12**, 917–930.
732 **Etienne-Manneville, S.** (2013). Microtubules in cell migration. *Annu. Rev. Cell Dev. Biol.* **29**, 471–499.
733 **Etienne-Manneville, S. and Hall, A.** (2001). Integrin-mediated activation of Cdc42 controls cell polarity
734 in migrating astrocytes through PKCζ. *Cell* **106**, 489–498.
735 **Hahn, I., Voelzmann, A., Liew, Y. T., Costa-Gomes, B. and Prokop, A.** (2019). The model of local
736 axon homeostasis - Explaining the role and regulation of microtubule bundles in axon maintenance
737 and pathology. *Neural Dev.* **14**, 1–28.
738 **Hurtado, L., Caballero, C., Gavilan, M. P., Cardenas, J., Bornens, M. and Rios, R. M.** (2011).
739 Disconnecting the Golgi ribbon from the centrosome prevents directional cell migration and
740 ciliogenesis. *J. Cell Biol.* **193**, 917–33.
741 **Kruse, R., Krantz, J., Barker, N., Coletta, R. L., Rafikov, R., Luo, M., Højlund, K., Mandarino, L.**
742 **J. and Langlais, P. R.** (2017). Characterization of the CLASP2 protein interaction network
743 identifies SOGA1 as a microtubule-associated protein. *Mol. Cell. Proteomics* **16**, 1718–1735.
744 **Kupfer, A., Louvard, D. and Singer, S. J.** (1982). Polarization of the Golgi apparatus and the
745 microtubule-organizing center in cultured fibroblasts at the edge of an experimental wound. *Proc.*
746 *Natl. Acad. Sci. U. S. A.* **79**, 2603–2607.
747 **Meiring, J. C. M., Shneyer, B. I. and Akhmanova, A.** (2020). Generation and regulation of microtubule

748 network asymmetry to drive cell polarity. *Curr. Opin. Cell Biol.* **62**, 86–95.

749 **Miller, P. M., Folkmann, A. W., Maia, A. R. R., Efimova, N., Efimov, A. and Kaverina, I.** (2009).
750 Golgi-derived CLASP-dependent microtubules control Golgi organization and polarized trafficking
751 in motile cells. *Nat. Cell Biol.* **11**, 1069–80.

752 **Mogensen, M. M., Tucker, J. B. and Stebbings, H.** (1989). Microtubule polarities indicate that
753 nucleation and capture of microtubules occurs at cell surfaces in Drosophila. *J. Cell Biol.* **108**,
754 1445–1452.

755 **Muroyama, A. and Lechler, T.** (2017). Microtubule organization, dynamics and functions in
756 differentiated cells. *Dev.* **144**, 3012–3021.

757 **Nishita, M., Satake, T., Minami, Y. and Suzuki, A.** (2017). Regulatory mechanisms and cellular
758 functions of non-centrosomal microtubules. *J. Biochem.* **109**, 20029–20034.

759 **Oddoux, S., Zaal, K. J., Tate, V., Kenea, A., Nandkeolyar, S. A., Reid, E., Liu, W. and Ralston, E.**
760 (2013). Microtubules that form the stationary lattice of muscle fibers are dynamic and nucleated at
761 golgi elements. *J. Cell Biol.* **203**, 205–213.

762 **Pepperkok, R., Bre, M. H., Davoust, J. and Kreis, T. E.** (1990). Microtubules are stabilized in
763 confluent epithelial cells but not in fibroblasts. *J. Cell Biol.* **111**, 3003–3012.

764 **Rivero, S., Cardenas, J., Bornens, M. and Rios, R. M.** (2009). Microtubule nucleation at the cis-side of
765 the Golgi apparatus requires AKAP450 and GM130. *EMBO J.* **28**, 1016–1028.

766 **Satake, T., Yamashita, K., Hayashi, K., Miyatake, S., Tamura-Nakano, M., Doi, H., Furuta, Y.,**
767 **Shioi, G., Miura, E., Takeo, Y. H., et al.** (2017). MTCL1 plays an essential role in maintaining
768 Purkinje neuron axon initial segment. *EMBO J.* **36**, 1227–1242.

769 **Sato, Y., Akitsu, M., Amano, Y., Yamashita, K., Ide, M., Shimada, K., Yamashita, A., Hirano, H.,**
770 **Arakawa, N., Maki, T., et al.** (2013). The novel PAR-1-binding protein MTCL1 has crucial roles
771 in organizing microtubules in polarizing epithelial cells. *J. Cell Sci.* **126**, 4671–4683.

772 **Sato, Y., Hayashi, K., Amano, Y., Takahashi, M., Yonemura, S., Hayashi, I., Hirose, H., Ohno, S.**
773 **and Suzuki, A.** (2014). MTCL1 crosslinks and stabilizes non-centrosomal microtubules on the
774 Golgi membrane. *Nat. Commun.* **5**, 5266.
775 **Tanaka, J., Miwa, Y., Miyoshi, K., Ueno, A. and Inoue, H.** (1999). Construction of Epstein-Barr virus-
776 based expression vector containing mini-oriP. *Biochem. Biophys. Res. Commun.* **264**, 938–43.
777 **Vorobjev, I. A. and Nadezhdina, E. S.** (1987). The Centrosome and Its Role in the Organization of
778 Microtubules. *Int. Rev. Cytol.* **106**, 227–293.
779 **Wei, J. H. and Seemann, J.** (2010). Unraveling the Golgi ribbon. *Traffic* **11**, 1391–1400.
780 **Wu, J. and Akhmanova, A.** (2017). Microtubule-Organizing Centers. *Annu. Rev. Cell Dev. Biol.* **33**,
781 annurev-cellbio-100616-060615.
782 **Wu, J., de Heus, C., Liu, Q., Bouchet, B. P., Noordstra, I., Jiang, K., Hua, S., Martin, M., Yang, C.,**
783 **Grigoriev, I., et al.** (2016). Molecular Pathway of Microtubule Organization at the Golgi
784 Apparatus. *Dev. Cell* **39**, 44–60.
785 **Yadav, S., Puri, S. and Linstedt, A. D.** (2009). A primary role for golgi positioning in directed
786 secretion, cell polarity, and wound healing. *Mol. Biol. Cell* **20**, 1728–1736.
787 **Yang, C., Wu, J., de Heus, C., Grigoriev, I., Liv, N., Yao, Y., Smal, I., Meijering, E., Klumperman,**
788 **J., Qi, R. Z., et al.** (2017). EB1 and EB3 regulate microtubule minus end organization and Golgi
789 morphology. *J. Cell Biol.* **216**, 3179–3198.
790

Figure 1

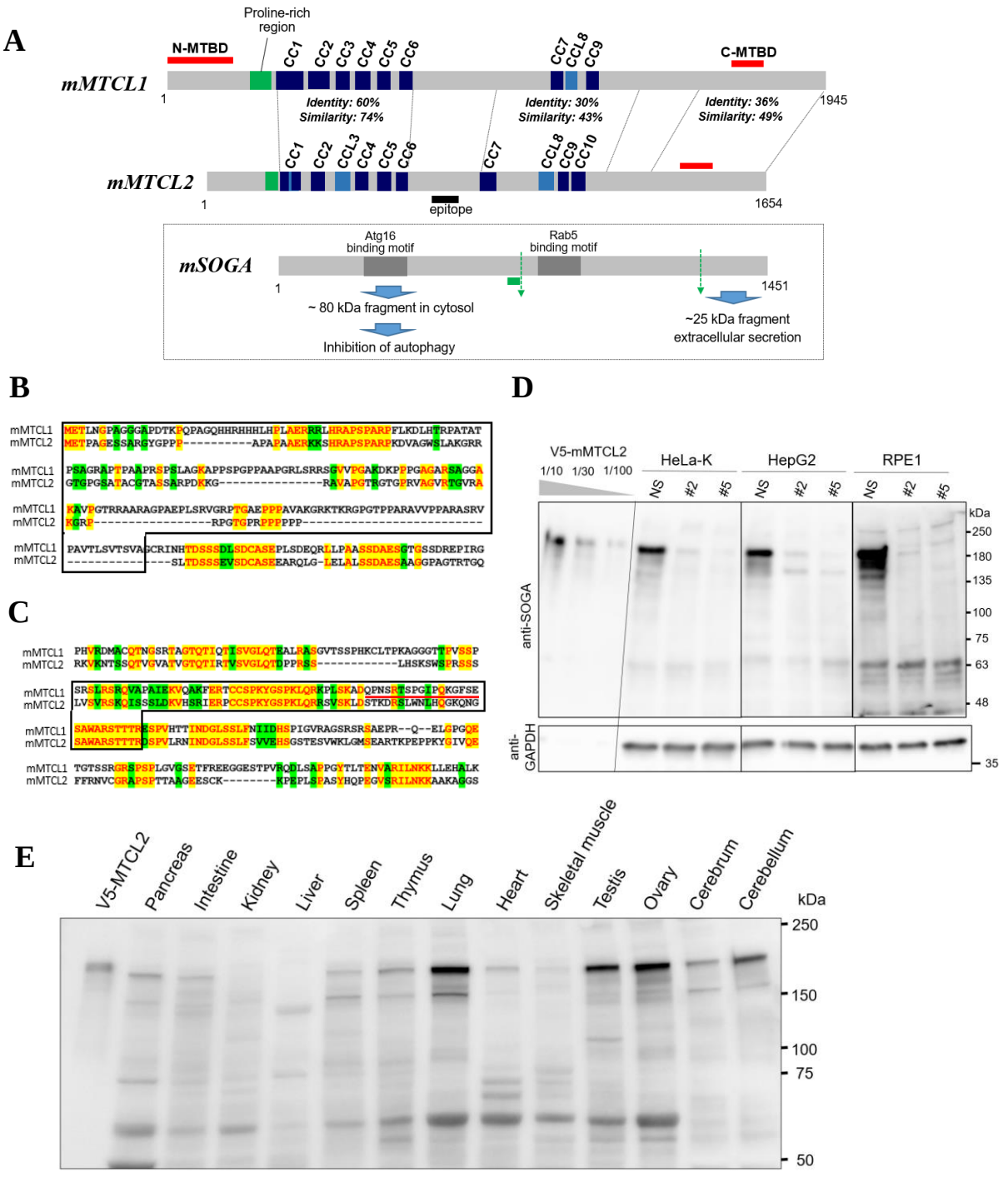
A
Proline-rich region
N-MTBD
C-MTBD
CC1
CC2
CC3
CC4
CC5
CC6
CC7
CCL8
CC9
mMTCL1
1
1945
Identity: 60%
Similarity: 74%
Identity: 30%
Similarity: 43%
Identity: 36%
Similarity: 49%
CCL3
CC10
mMTCL2
1654
epitope
Atg16 binding motif
Rab5 binding motif
mSOGA
1451
~ 80 kDa fragment in cytosol
Inhibition of autophagy
~25 kDa fragment extracellular secretion
B
mMTCL1
mMTCL2
C
D
V5-mMTCL2
1/10 1/30 1/100
HeLa-K
HepG2
RPE1
NS
#2
#5
anti-SOGA
anti-GAPDH
kDa
250
180
135
100
75
63
48
35
E
V5-MTCL2
Pancreas
Intestine
Kidney
Liver
Spleen
Thymus
Lung
Heart
Skeletal muscle
Testis
Ovary
Cerebrum
Cerebellum
kDa
250
150
100
75
50

Figure 2

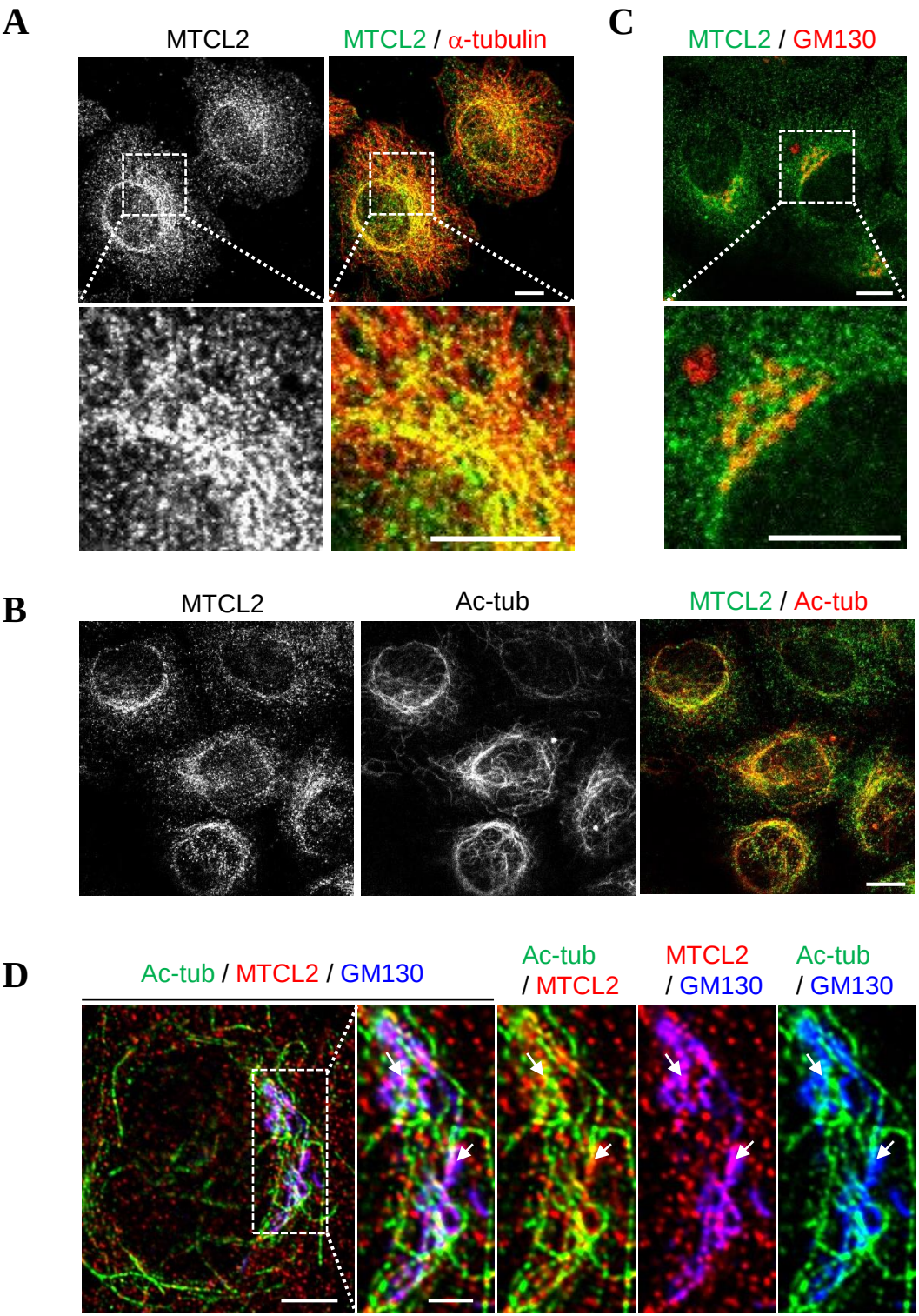
A
MTCL2
MTCL2 / α-tubulin
C
MTCL2 / GM130
B
MTCL2
Ac-tub
MTCL2 / Ac-tub
D
Ac-tub / MTCL2 / GM130
Ac-tub / MTCL2
MTCL2 / GM130
Ac-tub / GM130

Figure 3

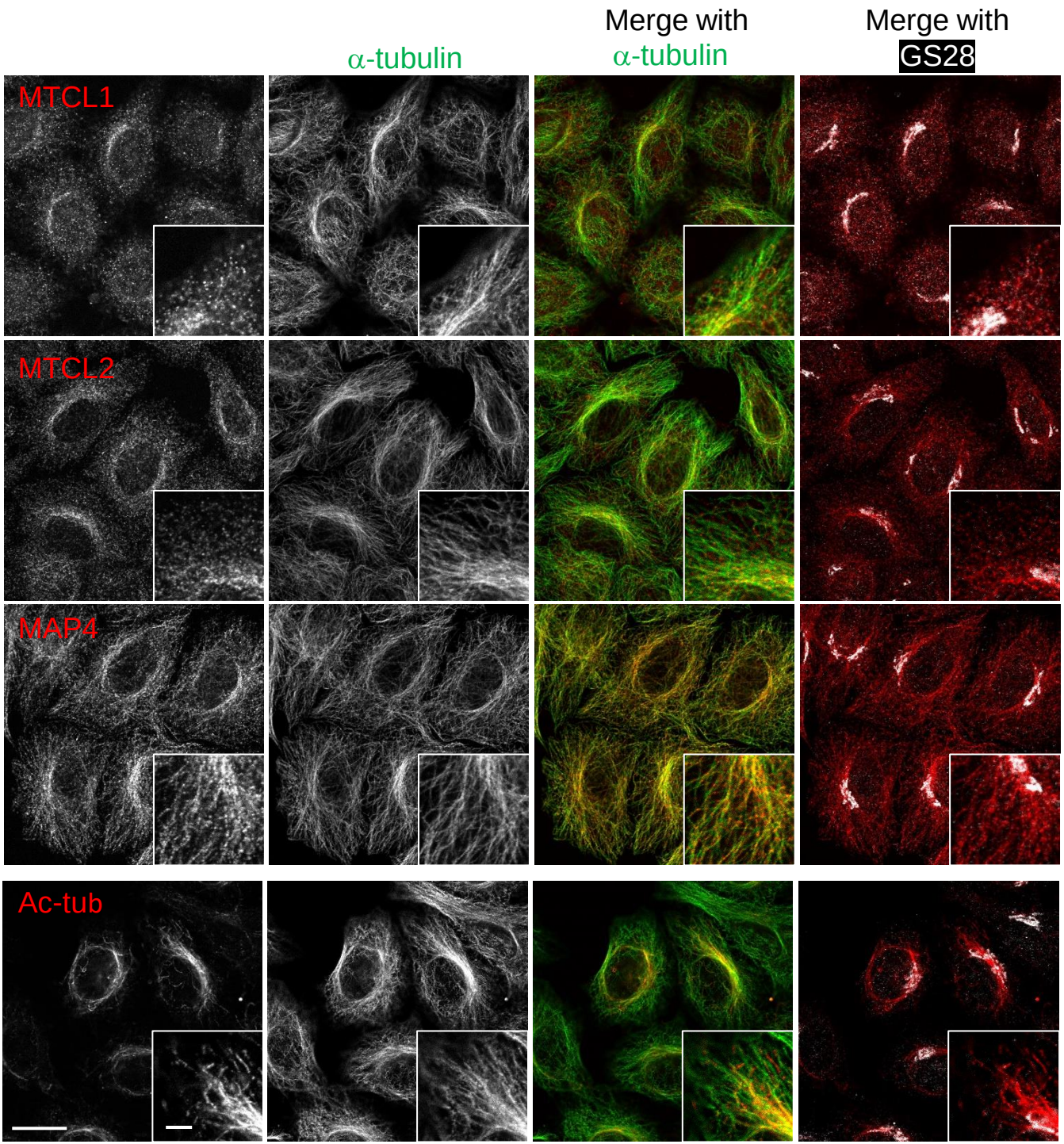
α-tubulin
Merge with α-tubulin
Merge with GS28
MTCL1
MTCL2
MAP4
Ac-tub

Figure 4

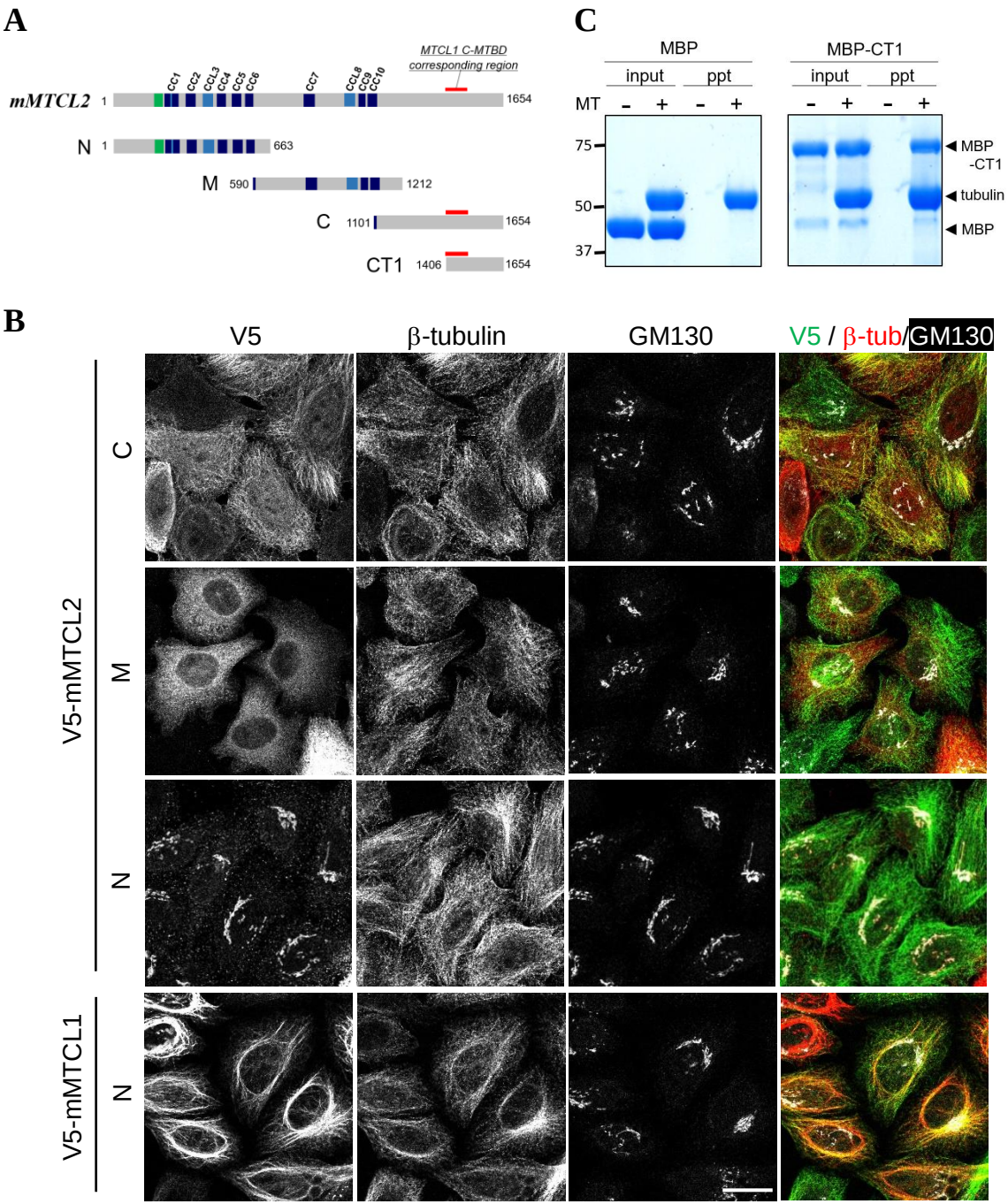
A
MTCL1 C-MTBD corresponding region
CC1
CC2
CCL3
CC4
CC5
CC6
CC7
CC8
CC9
CC10
mMTCL2 1 1654
N 1 663
M 590 1212
C 1101 1654
CT1 1406 1654
C
MBP
MBP-CT1
input
ppt
input
ppt
MT - + - + - + - +
75
50
37
MBP -CT1
tubulin
MBP
B
V5
β-tubulin
GM130
V5 / β-tub/GM130
V5-mMTCL2
C
M
N
V5-mMTCL1
N

Figure 5

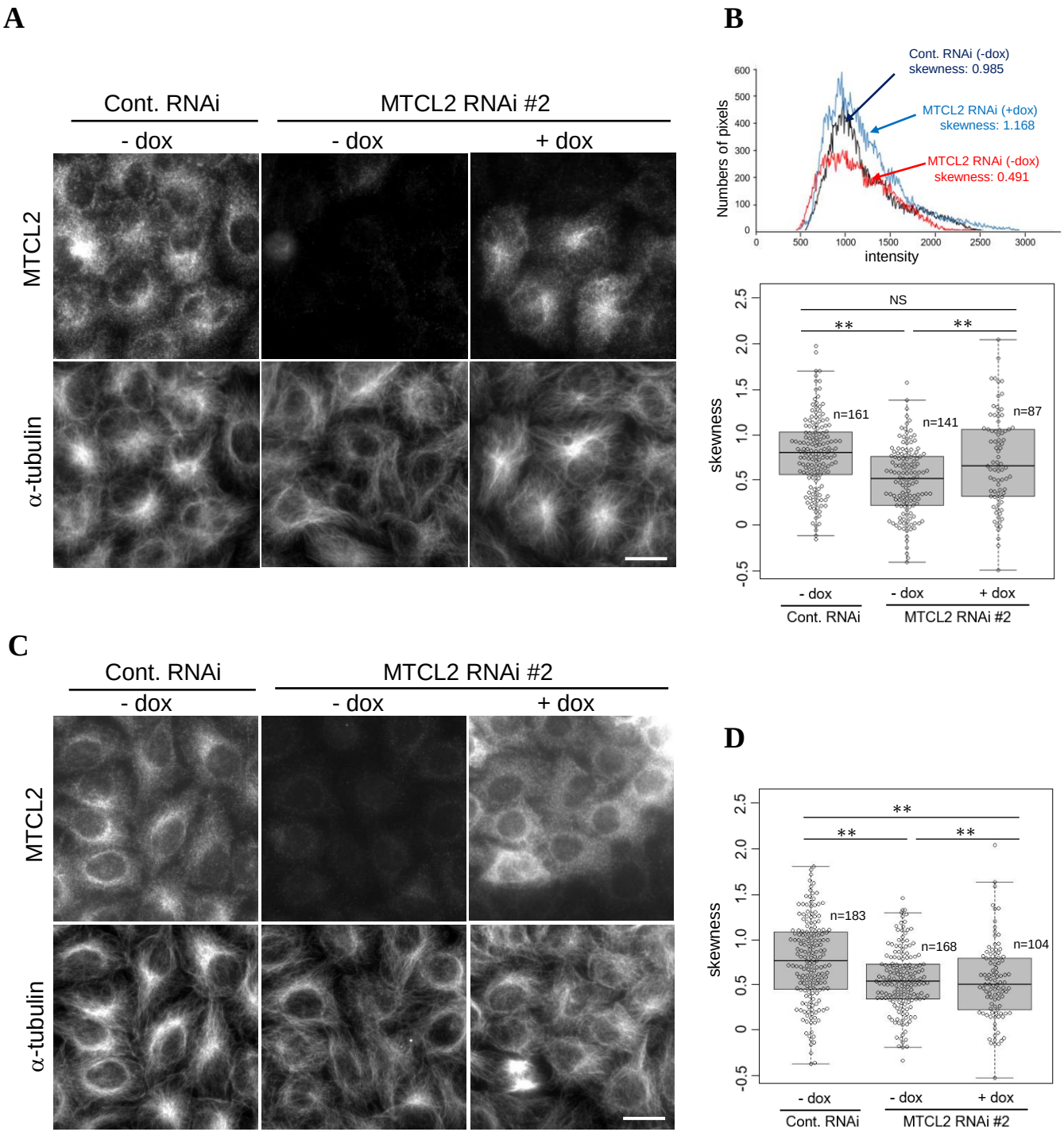
A
Cont. RNAi
MTCL2 RNAi #2
- dox
- dox
+ dox
MTCL2
α-tubulin
B
Cont. RNAi (-dox)
skewness: 0.985
MTCL2 RNAi (+dox)
skewness: 1.168
MTCL2 RNAi (-dox)
skewness: 0.491
Numbers of pixels
intensity
NS
**
**
n=161
n=141
n=87
skewness
- dox
- dox
+ dox
Cont. RNAi
MTCL2 RNAi #2
C
Cont. RNAi
MTCL2 RNAi #2
- dox
- dox
+ dox
MTCL2
α-tubulin
D
**
**
**
n=183
n=168
n=104
skewness
- dox
- dox
+ dox
Cont. RNAi
MTCL2 RNAi #2

Figure 6

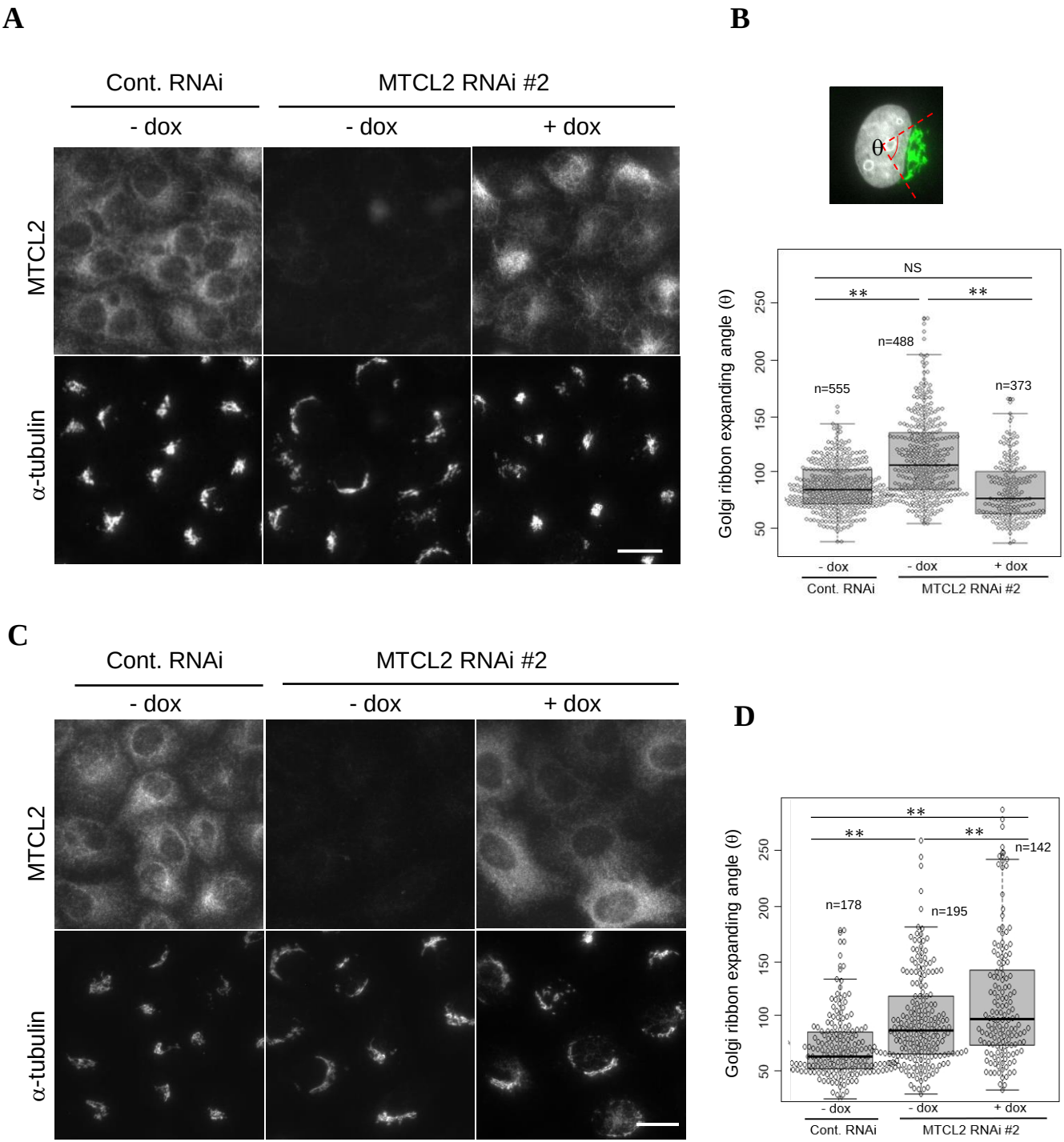
A
Cont. RNAi
MTCL2 RNAi #2
- dox
- dox
+ dox
MTCL2
α-tubulin
B
θ
NS
**
**
n=555
n=488
n=373
Golgi ribbon expanding angle (θ)
50
100
150
200
250
- dox
- dox
+ dox
Cont. RNAi
MTCL2 RNAi #2
C
Cont. RNAi
MTCL2 RNAi #2
- dox
- dox
+ dox
MTCL2
α-tubulin
D
**
**
**
n=178
n=195
n=142
Golgi ribbon expanding angle (θ)
50
100
150
200
250
- dox
- dox
+ dox
Cont. RNAi
MTCL2 RNAi #2

Figure 7

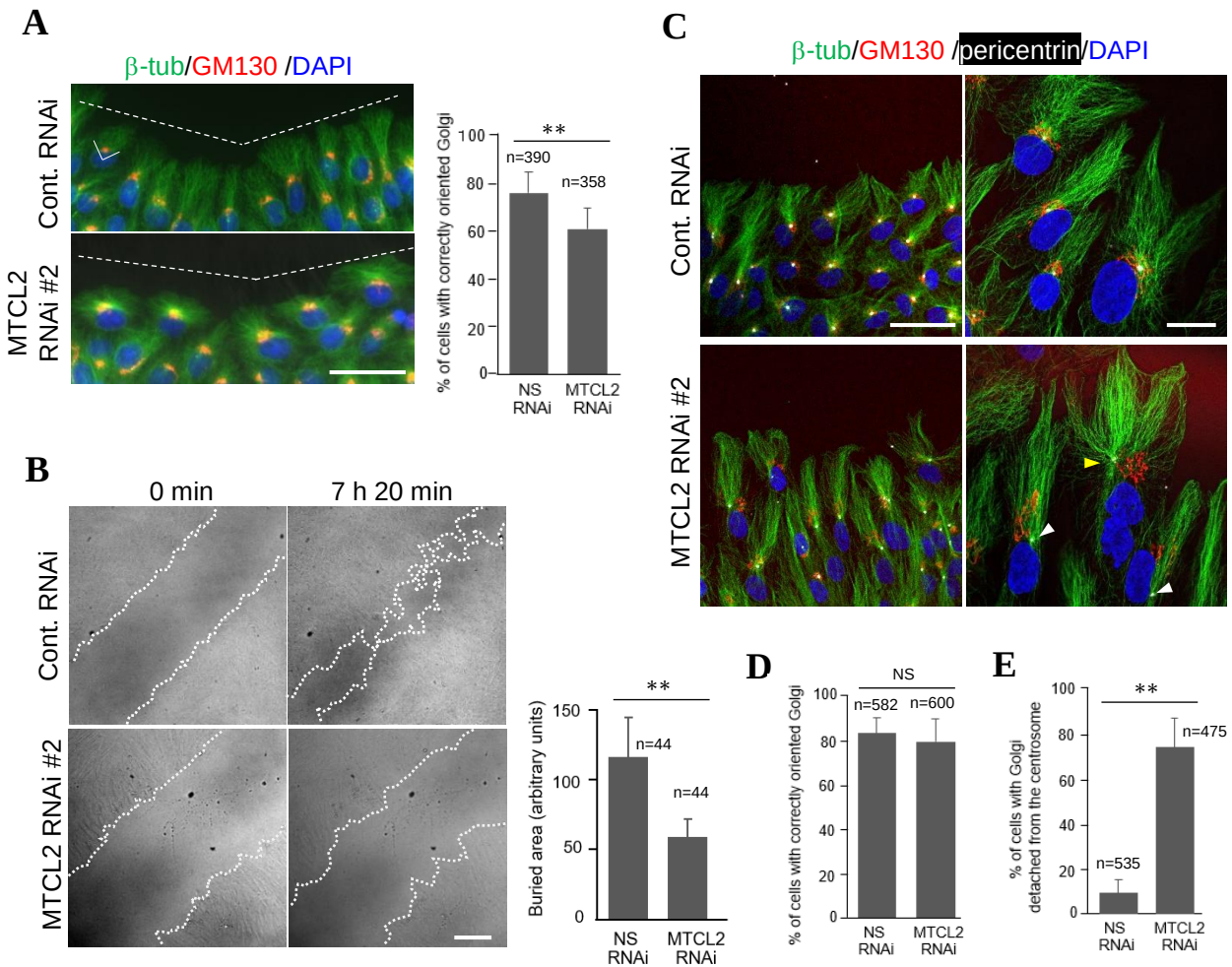
A
β-tub/GM130 /DAPI
Cont. RNAi
MTCL2 RNAi #2
% of cells with correctly oriented Golgi
**
n=390
n=358
NS RNAi
MTCL2 RNAi
B
0 min
7 h 20 min
Cont. RNAi
MTCL2 RNAi #2
Buried area (arbitrary units)
**
n=44
n=44
NS RNAi
MTCL2 RNAi
C
β-tub/GM130 /pericentrin/DAPI
Cont. RNAi
MTCL2 RNAi #2
D
NS
n=582
n=600
% of cells with correctly oriented Golgi
NS RNAi
MTCL2 RNAi
E
**
n=535
n=475
% of cells with Golgi detached from the centrosome
NS RNAi
MTCL2 RNAi

Figure 8

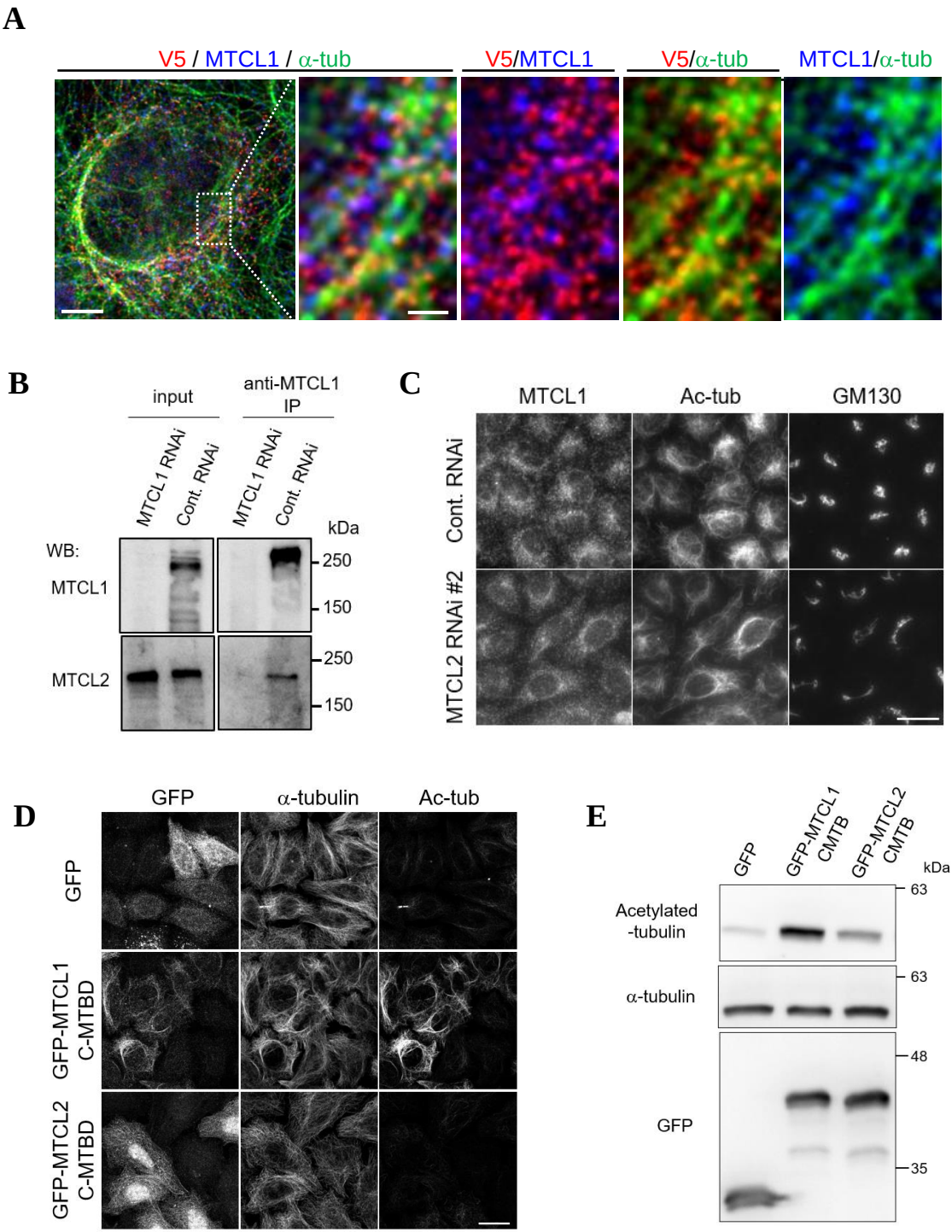
A
V5 / MTCL1 / α-tub
V5/MTCL1
V5/α-tub
MTCL1/α-tub
B
input
anti-MTCL1 IP
MTCL1 RNAi
Cont. RNAi
MTCL1 RNAi
Cont. RNAi
kDa
WB:
MTCL1
250
150
MTCL2
250
150
C
MTCL1
Ac-tub
GM130
Cont. RNAi
MTCL2 RNAi #2
D
GFP
α-tubulin
Ac-tub
GFP
GFP-MTCL1 C-MTBD
GFP-MTCL2 C-MTBD
E
GFP
GFP-MTCL1 CMTB
GFP-MTCL2 CMTB
kDa
Acetylated -tubulin
63
α-tubulin
63
48
GFP
35

Figure 9

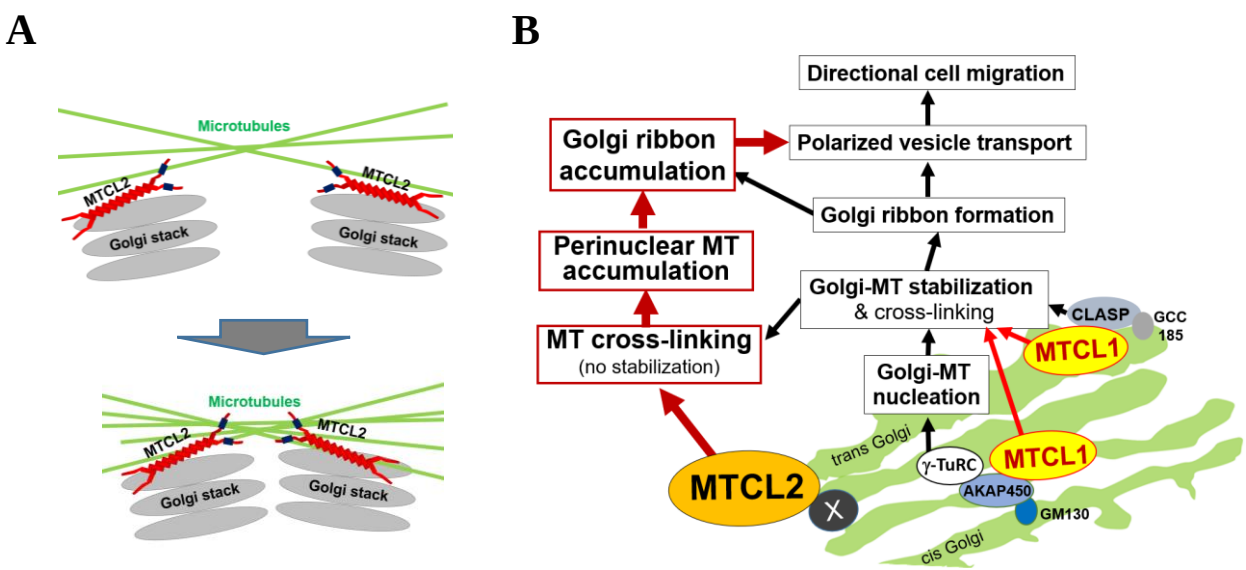
A
Microtubules
MTCL2
MTCL2
Golgi stack
Golgi stack
Microtubules
MTCL2
MTCL2
Golgi stack
Golgi stack
B
Directional cell migration
Golgi ribbon accumulation
Polarized vesicle transport
Golgi ribbon formation
Perinuclear MT accumulation
Golgi-MT stabilization & cross-linking
CLASP
GCC 185
MTCL1
MT cross-linking (no stabilization)
Golgi-MT nucleation
trans Golgi
γ-TuRC
MTCL1
MTCL2
X
AKAP450
GM130
cis Golgi